Downwelling over the Southern California Shelf

CLINTON D. WINANT

Scripps Institution of Oceanography, La Jolla, CA 92093

(Manuscript received 14 August 1979, in final form 6 December 1979)

ABSTRACT

Coastal downwelling events, induced by tropical storms which travel up along the coast, occur regularly during the summer over the shelf of Southern California. Large vertical velocities (0.5 cm s^{-1}) are observed over the very narrow (3.6 km) shelf. Simultaneous observations of longshore current and cross-shelf pressure gradient indicate the cross-shelf momentum balance is geostrophic. Heat balance computations reveal that the increase in mean temperature over the shelf is mostly caused by cross-shelf advection of heat. Large longshore accelerations occurring simultaneously at all depths in the shallower part of the shelf may be explained by longshore sea surface slopes contributing, along with the wind stress, to the longshore momentum balance. Profiles of temperature and velocity are consistent with a two-layer description of the vertical structure, these layers being separated by a thin, turbulent mixing layer.

1. Introduction

The coastal motions reported here are those which develop over the narrow southern California shelf when tropical storms pass by, traveling to the north along the coast of Baja California (Mexico) and Southern California. These are regular events which occur once or twice almost every year, between mid and late summer. The weather systems are weakening by the time they reach San Diego, but peak wind speeds are well in excess of 10 m s^{-1}, to the north. As a result a downwelling situation develops over the shelf, which bears some similarity to the upwelling motions which have been reported recently [cf. the reviews of Niiler (1975) and Winant (1979, 1980)].

The objective of this report is to document the observations of current, temperature and bottom pressure, and present budgets of heat and momentum constructed from these. Two different approaches exist where dynamical interpretations of observed coastal motions are concerned: a continuous time series approach covering periods of several months and a discrete approach, focused on a single wind stress event. Practically the event approach is usually selected when the period of high wind stress is an infrequent occurrence, or strong enough that dynamics during the event are expected to be notably different from those which obtain at other times, as in reports of hurricane-induced motions over the Gulf of Mexico (Forristall *et al.*, 1976; Smith, 1978). When the longshore wind stress is a sustained feature as it can be for instance off the coasts of Washington-Oregon, Peru or northeast Africa, a continuous analysis of the data (e.g., Allen and Kundu, 1978; Huyer *et al.*, 1978) may be preferable. Because the present report is concerned with the occurrence of single, well-defined wind features, the event approach is adopted.

2. The observations

Between August 1977 and March 1979 arrays of Vector Measuring Current Meters (VMCM) were deployed on the narrow shelf which separates Southern California from the Gulf of Catalina. The shelf (Fig. 1) has a fairly steep and practically constant slope (1.6×10^{-2}) and offshore of the shelf break, the slope increases to a value near 1.

The VMCM instrument was designed to measure accurate averages of currents in the presence of a large surface wave field. Extensive tow tank tests (Weller, 1978) and intercomparison studies (Winant *et al.*, 1978) confirm that resulting measurements have maximum errors on the order of 1 or 2 cm s^{-1}. The current meters are equipped to measure two components of the horizontal current and temperature, and they are deployed on a cross-shelf transect (Fig. 2) near Del Mar, California, 20 km to the north of San Diego, on separate moorings in 15, 30 and 60 m of water.

In all cases the current meters are distributed evenly in the vertical, the top instrument moored as close to the surface as possible on subsurface moorings. The 60 m mooring is just shoreward of the shelf break. In addition to the VMCM's, two bottom pressure transducers are deployed along the same shelf transect, one in 12 m water depth and the other in 30 m. All the instrumentation is set to record 2 min averages of the quantities observed. The corresponding Nyquist frequency is higher than

0022-3670/80/050791-09$06.25

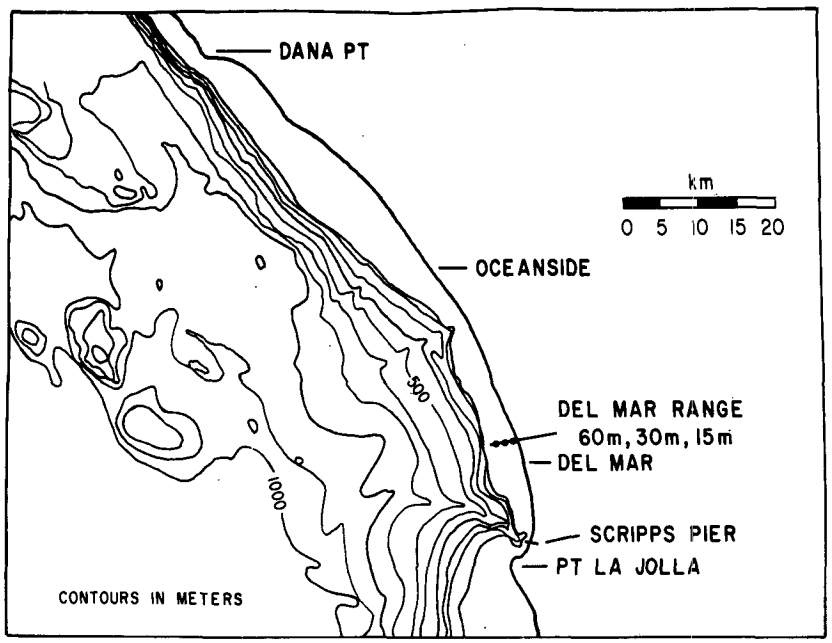

FIG. 1. The experimental site, along the coast of Southern California. Contour lines are in 100 m increments.

the highest buoyancy frequency occurring in summertime, and essentially in the middle of the spectral valley which separates the internal wave from the surface wave part of the energy spectrum.

The regular passage of a tropical storm along this coast during the summertime has been noted. The tracks of Doreen (17 August 1977) and Norman (5 September 1978) are shown in Fig. 3. These systems induced strong local winds, and in both cases instruments were deployed along the Del Mar rangeline recording the response of the shelf waters. Because the forcing in both instances was similar, and because more instruments were deployed during the second storm, the remainder of this report is devoted to the second storm. The results presented here are confirmed in all regards by the observations during the passage of the first storm.

The most dramatic reflection of the storm's passage and the resulting downwelling is provided by the temperature measurements at the 60 m station (Fig. 4). During the two weeks preceding the storm, the thermal structure over the shelf consists generally of an upper, warm (20°C) layer some 10 m in depth, beneath which the water temperature de-

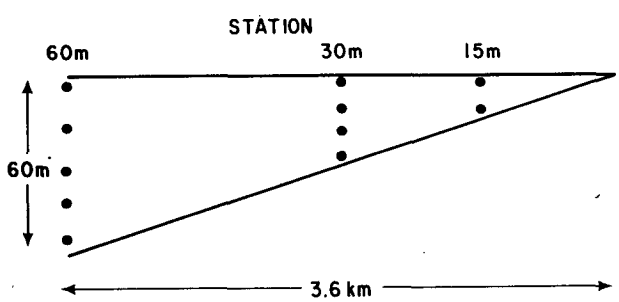

FIG. 2. Cross-shelf section at Del Mar, California, showing the current meter locations.

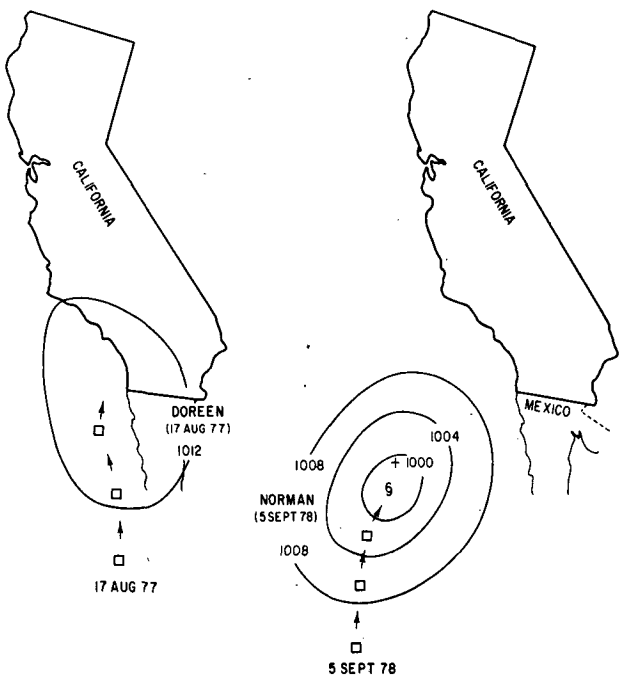

FIG. 3. Tracks of tropical storms Doreen (17 August 1977) and Norman (5 September 1978) as they traveled along the western seaboard of North America.

creases to 12°C over a depth of 10 m, and then remains essentially constant. Diurnal and semidiurnal temperature fluctuations are present. They are largest where the temperature gradient is largest, near the surface. For three days before the storm passed by Del Mar, the upper layer either cooled off or became very shallow (the latter is more likely in view of the large tidal temperature fluctuations observed at the top current meter). With the onset of winds brought by the tropical storm, the water temperature increases at all depths, and the upper layer deepens rapidly, extending beneath the instrument moored 43 m beneath the surface.

Wind speed and direction were measured at a coastal station at San Onofre, some 60 km to the north of the current meter array, and the wind speed, wind direction and barometric pressure observations made at Lindbergh Field, San Diego, 20 km to the southeast of Del Mar are also available. In Fig. 5, the longshore component of wind speeds measured at San Onofre and Lindbergh Field are compared, along with the barometric pressure. The longshore direction is defined as being tangent to the coastline at the Del Mar site. The wind direction was stable during the period, and within 10° of the longshore direction. The wind speed measurements at the two stations are consistent: while the barometric pressure dipped to a minimum of 29.7 inches Hg at 1700[1] on 5 September, the wind velocity suddenly increased in the upcoast direction to a maximum value near 12 m s^{-1} and blew at velocities exceeding 7 m s^{-1} until 0400 on 6 September. In the analysis to be presented, wind speeds and directions from San Onofre are used to estimate the wind stress, using the usual formula depending on the square of the wind speed, with a drag coefficient taken as 1.3×10^{-3}.

[1] All times local standard.

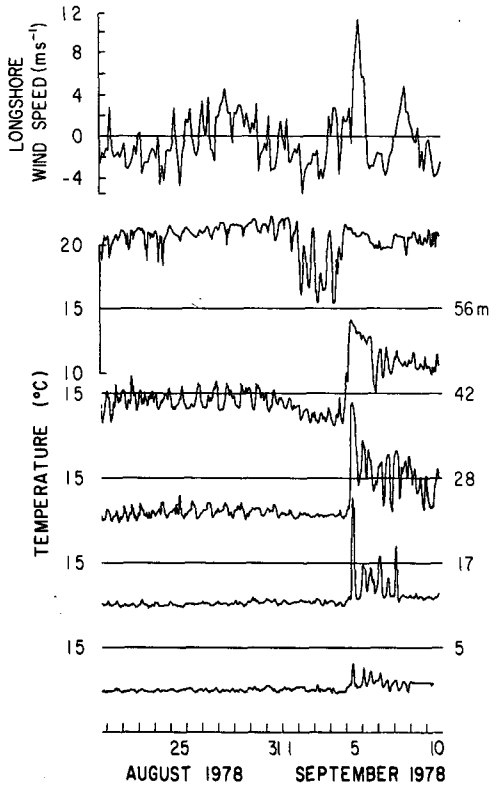

FIG. 4. Longshore wind speed and temperature observations at the 60 m station. The instrument height above the bottom is noted on the right-hand side.

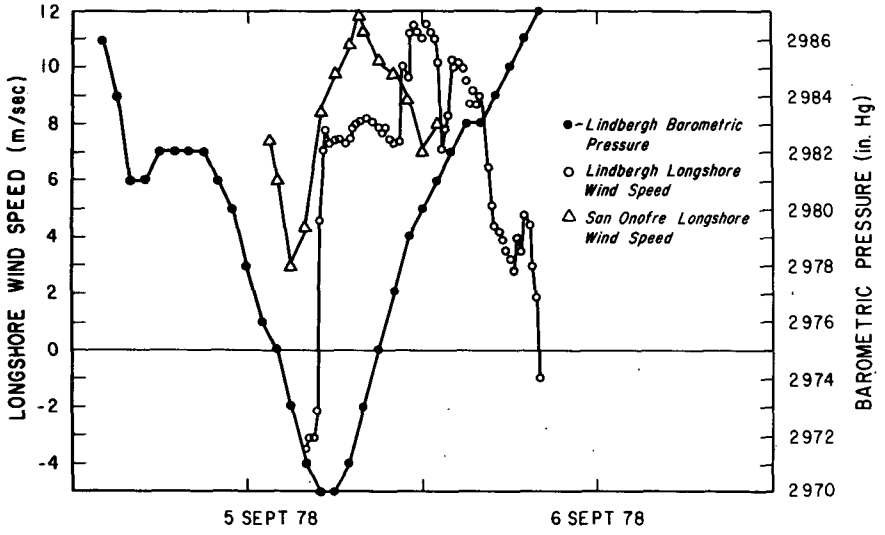

FIG. 5. Longshore wind speed reported from Lindbergh Field (San Diego) 20 km south of the experimental site and San Onofre 60 km north of the experimental site, along with the barometric pressure recorded at Lindbergh Field.

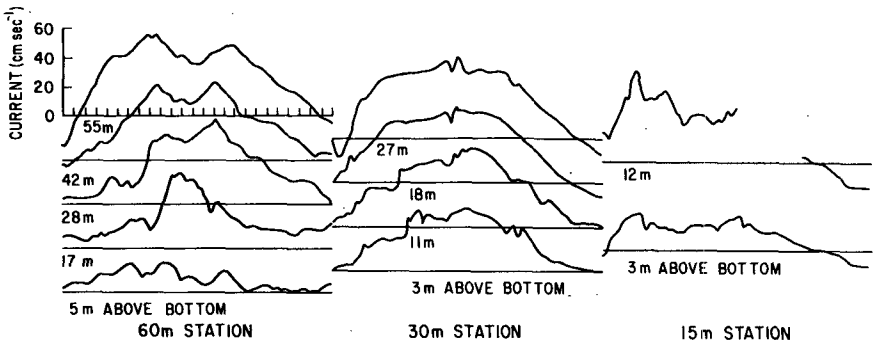

FIG. 6. Longshore current observations for each of the instruments deployed. The scales for each figure are similar to those shown for the top left-hand figure. Horizontal axis tick marks are 1 h apart.

Longshore currents measured by the current meter array are presented in Fig. 6, spanning a time period between 1600, 5 September and 1700, 6 September. The data presented in Fig. 6, as those presented in Figs. 7 and 8 are the unfiltered 2 min samples recorded by the VMCM instrument. The upper instrument at the 15 m station became fouled between 0500 and 1100 on 6 September. Initially, the upper layer at the 60 and 30 m stations is slowly drifting downcoast, but accelerates upcoast as soon as the wind begins to blow. The maximum acceleration depends on the exact depth of the observation, but ranges $\sim 5 \times 10^{-3}$ cm s^{-2} in the upper 5 m of water. The initial accelerations are observed, particularly at the 30 m station, to occur at all depths either at or very shortly after the onset of wind stress. Although a very large vertical diffusivity could account for this, an upcoast sea surface elevation gradient occurring synchronously with the wind stress is the more likely cause. The acceleration phase of the event ceases around 2200, 5 September, when the upper layer has reached speeds in excess of 50 cm s^{-1}, which prevail until 0800, 6 September, when the wind stress reverses and after which the upper layer decelerates.

Cross-shelf currents (Fig. 7) are more difficult to interpret. A 4 h lag separates the onset of wind stress from the acceleration of upper waters onshore, while the lower layer water is displaced offshore. Although the overall impression suggested by the cross-shelf velocities is generally consistent with the classical notion of downwelling, sudden reversals, such as those occurring near the middle of the record in the upper layer at the 30 m station, remain unexplained. Estimates of the vertically averaged cross-shelf velocity may be formed from weighted sums of the cross-shelf currents measured at any particular vertical array. A certain degree of arbitrariness is introduced since the vertical profile of velocity is not known between observation stations. In these calculations the velocity is assumed to vary linearly between any pair of current meters. The resulting vertically averaged cross-shelf velocity varies with amplitudes of order 1 cm s^{-1}. This amplitude is within experimental error of zero, and is also small relative to values at individual depths, so that to within experimental error, the volume balance appears to be two-dimensional.

Temperature measurements (Fig. 8) clearly illustrate the two-layer nature of the water column.

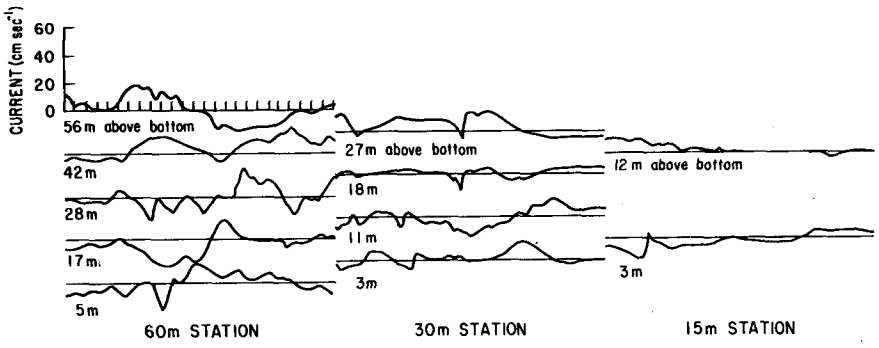

FIG. 7. Cross-shelf current observations for each of the instruments deployed. The scales for each figure are similar to those shown for the top left-hand figure. Horizontal axis tick marks are 1 h apart.

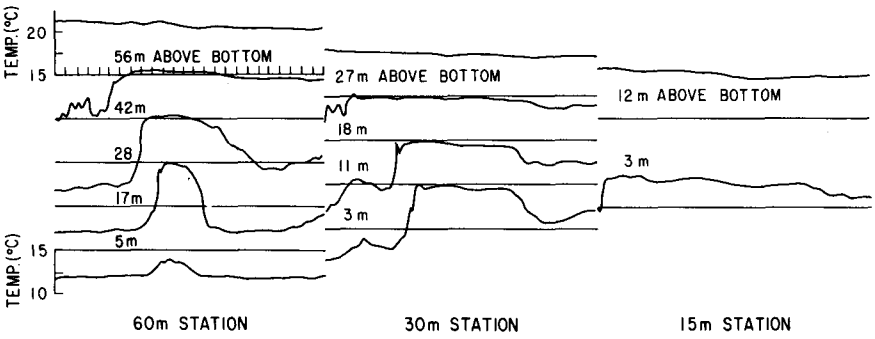

FIG. 8. Temperature observations for each of the instruments deployed. The scales for each figure are similar to those shown for the top left-hand figure. In each case the baseline corresponds to 15°C. Horizontal axis tick marks are 1 h apart.

While only the upper instruments initially register warm temperatures, the deepening of the upper layer is evident at depth as a sudden and large temperature change. There is a correlation between the temperature and longshore current observations: the sharp longshore acceleration which occurs 5 h after the beginning of the record, 18 m above the bottom at the 30 m station, is synchronous with the warming at the same depth. Thus the two layers differ not only in temperature, but also in momentum, so that the two-layer nature of the water column can be thought of as describing the vertical momentum structure as well as the vertical thermal structure. The temperature measurements are summarized in Fig. 9, where the depth of the 20°C isotherm is tracked at the 60 and 30 m stations. The upper layer deepens uniformly across the shelf, reaching a maximum descent rate of 0.5 cm s^{-1}.

Vertical motion induced either by downwelling or mixing will result in deepening of an isotherm. The relative importance of these competing influences may be roughly estimated as follows: if the downwelling process is essentially two dimensional, the rate of descent of the interface is $dh/dt = \tau/\rho fL$ if the cross-shelf velocity in the upper layer is estimated to be $\tau/\rho fH$ (L is the shelf width and H a measure of the upper layer thickness). The mixed-layer model of Pollard *et al.* (1973) results in a mixed-layer deepening rate $dh/dt = 2^{-3/4}(\tau/\rho Nt)^{1/2}$, where N is the buoyancy frequency associated with the interface beneath the mixed layer. Initially, then, the deepening is controlled by mixing, but after a time $t \approx 2^{-3/2}\rho f^2L^2/N\tau$ (for values typical of this downwelling event, this time is of order one hour), the deepening of an isotherm is controlled by the vertical velocity induced by the downwelling.

This estimate of vertical velocity may be checked by the following argument, based on the previous suggestion that the volume balance is essentially two-dimensional. A horizontal flux into a control surface bound by the bottom, the edge of the shelf and a horizontal line at some depth beneath the surface must be balanced by a vertical flux through the top boundary of the control surface. Consider the flux out of such a surface in 60 m of water, between the 17 m observation station and the bottom. The maximum offshore velocity (Fig. 7), at both 5 and 17 m above the bottom, is 20 cm s^{-1}. The horizontal extent of such a surface is 1 km so that vertical velocities are 0.34 cm s^{-1}, of the same order as those deduced from the deepening of the 20° isotherm.

Such values are considerably larger than typical values of vertical velocity reported in upwelling situations off the coasts of Oregon and Africa (Barton *et al.*, 1977) which range around 0.1 cm s^{-1}. Simple continuity considerations demonstrate that, other elements being equal, vertical velocities are inversely proportional to the shelf width, which off Southern California is close to being ten times less than that of Oregon. The vertical downwelling veloci-

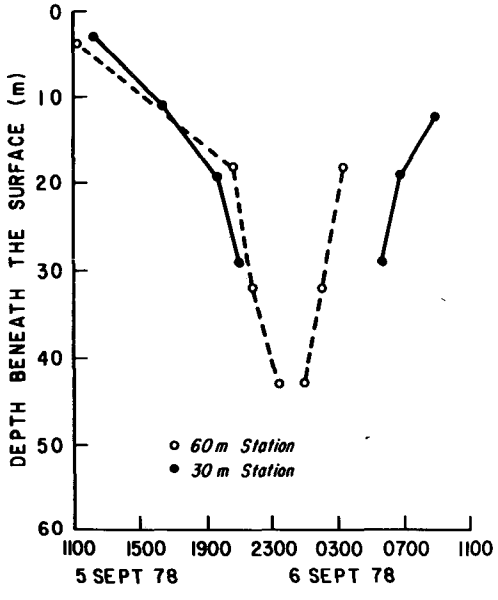

FIG. 9. Depth of the 20°C isotherm at the 60 m station (dashed line) and at the 30 m station (solid line).

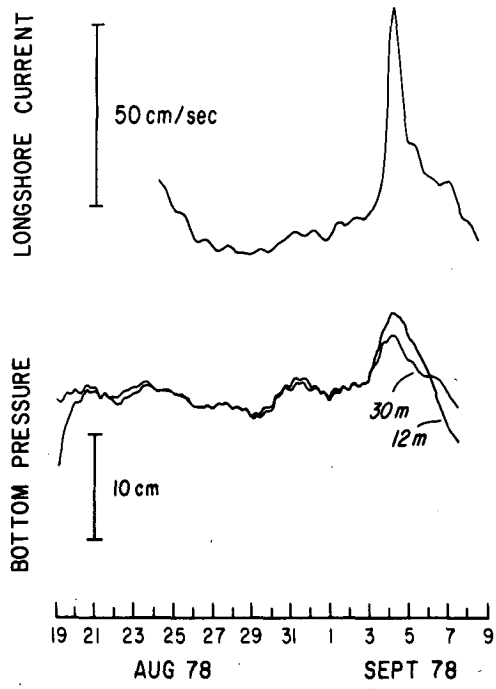

FIG. 10. De-tided bottom pressure signals at the 30 and 12 m stations along with the longshore current corresponding to the barotropic empirical mode.

ties described here are thus not inconsistent with prior observations of vertical upwelling velocities.

3. The cross-shelf momentum balance

We adopt a coordinate system in which the x axis points onshore, the y axis alongshore and the z axis upward with origin at the mean sea level. The bottom is given by $z = -H(x,y)$ and the free surface by $z = \eta$. The linearized cross-shelf component of the momentum equation is

$$u_t - fv = -p_x/\rho \tag{1}$$

in the absence of friction. If this equation is integrated vertically from the bottom of the surface, it becomes

$$U_t - fV = -\int_{-H}^{\eta} p_x \rho^{-1} dz, \tag{2}$$

where

$$U,V = \int_{-H}^{\eta} (u,v) dz.$$

If the density difference between the two layers is neglected and the vertical momentum balance taken to be hydrostatic

$$p = \rho g(\eta - z),$$

Eq. (2) becomes

$$U_t - fV = -g(\eta + H)\eta_x. \tag{3}$$

Most models of coastal circulation neglect the term U_t in (3) although as changes in V occur, U_t may take on nonzero values. It is simple to show, however, that sea surface elevation gradients η_x set up very rapidly to balance fV. The time required for such adjustments is just the time a surface gravity wave takes to cross the shelf, when the shelf is narrower than the external Rossby radius of deformation. In the present instance, with a shelf width of 3.6 km and a mean depth of 30 m, this time is of order 200 s. In these observations the vertically averaged cross-shelf velocity estimated from the data varies with amplitudes of order 1 cm s^{-1}, as noted in Section 2. Since these values are of the same order as the expected errors in the measurements, it must be concluded that U is small enough that it cannot be determined, but at any rate is smaller than fV by at least an order of magnitude.

In Fig. 10, records from both bottom pressure sensors in 12 and 30 m of water are presented along with a barotropic longshore velocity over the shelf. The bottom pressure records were low-pass filtered with a filter whose half-power point was set at a 1-day period in order to remove the tidal fluctuations. The barotropic longshore velocity is obtained by an empirical orthogonal function analysis of the longshore velocities measured by each instrument in the current meter array over the entire deployment period (27 July–13 September 1978). This eigenfunction accounts for 44% of the variance in the data set while a baroclinic eigenfunction accounts for 39% of the variance. The velocity distribution corresponding to the barotropic eigenfunction is roughly uniform in depth at each station, with larger velocities characterizing the offshore observations.

The data in Fig. 10 show the bottom pressure to rise synchronously with the onset of the longshore motion, the amplitude of the pressure response is greater in shallower water and thus a pressure gradient exists in the proper direction to balance the coriolis term in Eq. (3). With $f = 10^{-4}$ s^{-1} and $V = 1.5 \times 10^5$ cm^2 s^{-1}, the latter may be estimated to have a maximum value of 15 cm^2 s^{-2}. Estimating the pressure gradient from the data of Fig. 10 is more difficult, because of errors involved in the bottom pressure records. These errors are estimated to be on the order of 0.5 cm so that the maximum pressure difference is 2 cm ± 1 cm. This corresponds to a pressure gradient of $2 \pm 1 \times 10^{-5}$ (the sensors are 1 km apart), and to a pressure gradient term in Eq. (3) of 60 ± 30 cm^2 s^{-2}. Although the data quality is insufficient to determine whether the proper balance is that which obtains when the U_t term is neglected in (3), there is a clear tendency for this to happen, as suggested by the observations on the Alaskan shelf reported by Hayes (1979). This result confirms the earlier suggestion that U is within experimental error of zero.

4. Budgets of heat and momentum

Because of the small cross-shore gradients during the spinup phase, the mean temperature $\bar{T}$ and the mean longshore current $\bar{v}$ on the shelf may be estimated from measurements at the 60 m station:

$$\bar{T} = \frac{1}{HL} \sum_{i=1}^{5} T_i h_i l_i, \tag{4}$$

$$\bar{v} = \frac{1}{HL} \sum_{i=1}^{5} v_i h_i l_i, \tag{5}$$

where T_i and v_i are the temperature and longshore current measured by the ith current meter, $h_i l_i$ is the area of height h_i and width l_i which the observations by the ith current meter typify, and HL is the cross-sectional area of the shelf. The time dependence of $\bar{T}$ is depicted in Fig. 11 and that of $\bar{v}$ in Fig. 12. The time dependence of $\bar{T}$ clearly demonstrates that the deepening of the upper layer is not simply a result of turbulent mixing as is the case in the deeper ocean, but is generally controlled by the advection of warmer water which increases the mean temperature on the shelf.

In the absence of heat fluxes from the atmosphere and the bottom (whose effect on the mean temperature is negligible on the time scale considered here), changes in $\bar{T}$ must be due to either cross-shelf or longshore temperature fluxes. In view of the experimental arrangement it is not possible to estimate the latter, but the former are simply estimated from the current meter and temperature fluctuations observed at the 60 m station. Imagine a two-dimensional control surface extending in the vertical from surface to bottom and in the cross-shelf direction from the beach to the 60 m station. If A is the cross-sectional area the time rate of change of mean temperature is given by

$$HL \frac{\partial \bar{T}}{\partial t} = \int_{-H}^{\eta} uTdz\Big|_{60\text{m}} \tag{6}$$

when heat fluxes at the surface, the bottom and in the longshore direction are ignored. Under these circumstances, the mean temperature on the shelf can be deduced from the measurements at the 60 m station as

$$\bar{T} - \bar{T}(t = 0) = \frac{1}{HL} \int_0^t \int_{-H}^{\eta} uTdzdt, \tag{7}$$

where $\bar{T}(t = 0)$ represents the mean temperature on the shelf at the beginning of the integration. The $\bar{T}$ computed in this way is compared to the $\bar{T}$ computed from Eq. (4) in Fig. 11. The agreement is good in the sense that the difference between the mean temperature computed in both ways is considerably smaller than the variation in $\bar{T}$. Based on this evidence we may conclude that longshore heat fluxes are relatively unimportant compared with cross-shelf fluxes in determining the mean temperature over the shelf.

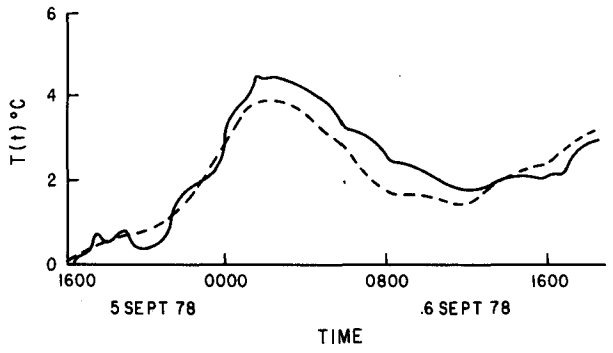

FIG. 11. Mean temperature $\bar{T}$ over the shelf as determined from Eq. (4) (solid line) and Eq. (7) (dashed line).

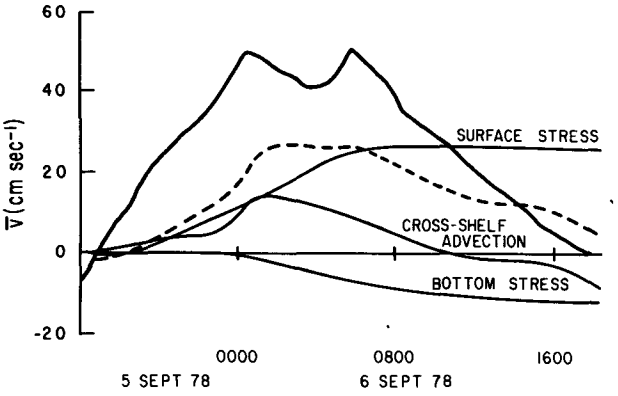

FIG. 12. Mean longshore velocity $\bar{v}$ over the shelf as determined from Eq. (5) (solid line) and Eq. (11) (dashed line). Light solid lines represent the individual contributions of different terms to the $\bar{v}$ computed using Eq. (11).

In attempting to construct budgets of longshore momentum in a similar way, it is necessary to incorporate estimates of surface and bottom stresses which clearly are not negligible. In addition, the effects of longshore fluxes of momentum and of longshore pressure gradients are *a priori* not known. If they were small, the rate of change of mean longshore velocity in the same control surface would be given by

$$A \frac{\partial \bar{v}}{\partial t} = \int_{-H}^{\eta} uvdz + \frac{L}{\rho}(\tau_s - \tau_b), \tag{8}$$

in which the first term on the right-hand side represents the cross-shelf flux of longshore velocity, and the second term is the difference between surface and bottom stress. Since neither of the latter two parameters are measured directly they are estimated, for present purposes, using the standard drag formula based on the square of the velocity:

$$\tau_s = \rho_a C_d w|w|, \tag{9}$$

$$\tau_b + \rho C_d v_b|v_b|, \tag{10}$$

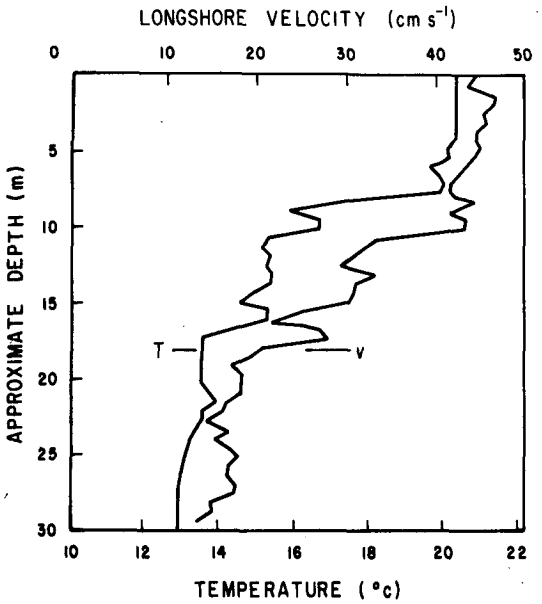

FIG. 13. Vertical profiles of temperature T and longshore velocity v obtained by assuming the vertical structure is advected down by the current meter 28 m above the bottom at the 60 m station at a constant vertical velocity of 0.5 cm s^{-1}.

where ρ_a is the air density, w the wind velocity and v_b an estimate of the longshore velocity above the bottom boundary layer. While the errors involved in using the first of these relations are fairly well understood (Garratt, 1976), it should be noted that the parameterization of the bottom stress used here, modeled directly after that of surface stress, is essentially unverified. For lack of any better information we use the same drag coefficient as that usually adopted for the surface stress ($C_d = 1.3 \times 10^{-3}$) and use the bottom current meter observations for v_b. A rough estimate of the log layer thickness is 1 m (Wimbush and Munk, 1971); the bottom current meter is 5 m above the bottom, well outside the log layer.

With all these approximations, Eq. (8) can be integrated to give an estimate of the mean longshore velocity on the shelf

$$\bar{v} - \bar{v}(t = 0) = \frac{1}{A}\int_0^t \left[\int_{-H}^{\eta} uv\,dz + \frac{L}{\rho}(\tau_s - \tau_b)\right]dt. \quad (11)$$

The mean velocity computed in this way is presented as a broken line in Fig. 12, along with the individual contribution of each term on the right-hand side of Eq. (11). The mean velocity computed using Eq. (5) is shown as a heavy solid line. Clearly, in this instance the agreement is not nearly as good as in the case of the mean temperature. Possible explanations for the discrepancy are the parameterization of bottom stress and the neglect of longshore momentum fluxes and longshore pressure gradients. During the acceleration phase of the events described here, between 1600 and 2400 on 5 September the velocities are relatively small, and the bottom stress (which depends on the square of the velocity) must also be relatively small. Errors in estimating this term cannot then have an important bearing in the momentum balance. It must be concluded that either the longshore momentum fluxes or pressure gradients play an important role in accelerating the alongshore flow.

5. Vertical stability and mixing

The time series of longshore velocity and temperature presented in Figs. 6 and 8 suggest that the thermal and momentum interfaces which separate the upper and lower layers are sharp. In a sense the situation which developed during this downwelling event, where the interface is advected vertically down by fixed instruments, is not unlike a laboratory situation in which instrumentation is traversed vertically through a mixing layer whose vertical position is fixed. The time series which are reported here may be loosely interpreted as vertical profiles of temperature and current, if the vertical depth is related to time as $z = wt$. As measured by the deepening of the 20°C isotherm, the vertical velocity was estimated to be 0.5 cm s^{-1}; on the basis of continuity arguments, it was estimated to be 0.3 cm s^{-1}. Although the precise value of the vertical velocity is not clear, it is of the order 0.5 cm s^{-1} and this value is used to draw vertical profiles of temperature and current in Fig. 13. The data are the unfiltered time series of temperature and longshore velocity replotted on an expanded time (or depth) scale, the values of depth on the horizontal axis being only approximate.

Because of the difficulties encountered in trying to obtain reliable estimates of vertical gradients based on such data, errors in estimating the Richardson number profiles are large. Nonetheless, the data exhibit a number of important features related to stability and mixing. The overall change in temperature across the interface is 7°C which corresponds to a relative density change $\Delta\rho/\rho$ of 1.4×10^{-3}. The overall velocity difference Δv is on the order of 30 cm s^{-1}, and a typical dimension h over which the gradients are spread is 10 m. An overall estimate of the Richardson number $\mathrm{Ri} = g\Delta\rho h/\rho\Delta v^2$ is thus of order 1. However, it is quite evident that very sharp gradients in temperature and in velocity exist, and these gradients are not necessarily coincident, so that areas of large velocity gradients are in all likelihood areas where mixing is taking place. The situation is reminiscent of laboratory experiments in which turbulent mixing is observed to eat away at a stable density interface. In this regard these observa-

tions complement those of Halpern (1976) who noted a strong tendency for instability and subsequent mixing to occur in an upwelling situation.

6. Conclusions

The observations reported here describe a somewhat incomplete dynamical picture of a strong downwelling event. While the motions are in general agreement with the usual qualitative descriptions of downwelling, questions arise as soon as attempts are made to quantitatively compare different dynamical terms in the equations of motion. The most serious limitation of the observations presented here concerns the lack of information on longshore gradients and particularly on the longshore sea surface elevation gradient.

Acknowledgments. The support of the National Science Foundation under Grant OCE 78-19295 is gratefully acknowledged. Helpful suggestions from K. H. Brink are appreciated.

REFERENCES

Allen, J. S., and P. K. Kundu, 1978: On the momentum, vorticity and mass balance on the Oregon shelf. *J. Phys. Oceanogr.*, **8,** 13–27.

Barton, E. D., A. Huyer and R. L. Smith, 1977: Temporal variation observed in the hydrographic regime near Cabo Corveiro in the northwest Africa upwelling region, February to April 1974. *Deep-Sea Res.*, **24,** 7–24.

Forristall, G. Z., R. C. Hamilton and V. G. Cardone, 1977: Continental shelf currents in tropical storm Delia, observations and theory. *J. Phys. Oceanogr.*, **7,** 532–546.

Garratt, J. R., 1977: Review of drag coefficients over ocean and continents. *Mon. Wea. Rev.*, **105,** 915–929.

Halpern, D., 1976: Structure of an upwelling event observed off Oregon during July 1973. *Deep-Sea Res.*, **23,** 495–508.

Hayes, S. P., 1979: Variability of current and bottom pressure across the continental shelf in the northeast Gulf of Alaska. *J. Phys. Oceanogr.*, **9,** 88–103.

Huyer, A., R. L. Smith and E. J. C. Sobey, 1978: Seasonal differences in low-frequency current fluctuations over the Oregon continental shelf. *J. Geophys. Res.*, **83,** 5077–5089.

Niiler, P. P., 1975: A report on the continental shelf circulation and coastal upwelling. *Rev. Geophys. Space Phys.*, **13,** 609–614.

Pollard, R. T., P. B. Rhines and R. O. R. Y. Thomson, 1973: The deepening of the wind mixed layer. *Geophys. Fluid Dyn.*, **4,** 381–404.

Smith, N. P., 1978: Longshore currents on the fringes of hurricane Anita. *J. Geophys. Res.*, **83,** 6047–6051.

Weller, R. A., 1978: Observations of horizontal velocity in the upper ocean made with a new Vector Measuring Current Meter. Ph.D. dissertation, University of California, San Diego, 169 pp.

Wimbush, M., and W. H. Munk, 1971: The benthic boundary layer. *The Sea,* Vol. 4, Wiley-Interscience, 731–758.

Winant, C. D., 1979: Coastal current observations. *Rev. Geophys. Space Phys.*, **17,** 89–98.

——, 1980: Coastal circulation and wind-induced currents. *Annual Review of Fluid Mechanics*, Vol. 12, Annual Reviews, Inc., 271–301.

——, R. E. Davis and R. A. Weller, 1978: Shallow current measurements. *Proc. Working Conference on Current Measurement*, Tech. Rep. DEL-SG-3-78, College of Marine Studies, University of Delaware, 372 pp.